Universal Logical Gates on Topologically Encoded Qubits via Constant-Depth Unitary Circuits

Guanyu Zhu, Ali Lavasani, and Maissam Barkeshli
Department of Physics, Condensed Matter Theory Center, University of Maryland, College Park, Maryland 20742, USA and Joint Quantum Institute, University of Maryland, College Park, Maryland 20742, USA

(Received 14 May 2019; accepted 8 July 2020; published 28 July 2020)

A fundamental question in the theory of quantum computation is to understand the ultimate space-time resource costs for performing a universal set of logical quantum gates to arbitrary precision. Here we demonstrate that non-Abelian anyons in Turaev-Viro quantum error correcting codes can be moved over a distance of order of the code distance, and thus braided, by a constant depth local unitary quantum circuit followed by a permutation of qubits. Our gates are protected in the sense that the lengths of error strings do not grow by more than a constant factor. When applied to the Fibonacci code, our results demonstrate that a universal logical gate set can be implemented on encoded qubits through a constant depth unitary quantum circuit, and without increasing the asymptotic scaling of the space overhead. These results also apply directly to braiding of topological defects in surface codes. Our results reformulate the notion of braiding in general as an effectively instantaneous process, rather than as an adiabatic, slow process.

DOI: 10.1103/PhysRevLett.125.050502

The possibility of a scalable universal quantum computer rests on quantum error correction and fault tolerance [1,2]. A promising class of quantum error correcting codes (QECCs) are topological QECCs, where the information is nonlocally encoded in a topologically ordered quantum state of matter [1–3]. For a QECC to allow fault-tolerant quantum computation, it must be possible to perform fault-tolerant logical gates on the encoded logical qubits, for example, via braiding of non-Abelian anyons, holes, or twist defects in topological QECCs [3–7]. Braiding of Fibonacci anyons in certain non-Abelian topological QECCs [4,5,8] can form a universal logical gate set [9–11].

Other proposed methods to realize a universal fault-tolerant gate set involve magic state distillation [12], code switching, or gauge fixing [13,14]. However, such methods necessarily carry a large space-time overhead depending on the code distance d, and all require measurements to achieve universality. It is an open question whether a universal logical gate set can be realized with just constant-depth unitary circuits independent of code distance d and requiring no measurements. In the context of topological codes, this question is also deeply related to a quantum complexity problem: the circuit complexity of unitary transformations between arbitrary states in the ground-state subspace of topologically ordered systems. Topologically ordered states are nontrivial phases of matter, which implies that a unitary circuit composed of few-qubit gates with depth of $\mathcal{O}(\log d)$ is needed to prepare the ground states from a trivial product state [15,16]. Naively one may expect that the transformation between two arbitrary ground states will also need at least a $\mathcal{O}(\log d)$-depth unitary circuit using a path connecting both states and going through the trivial product state in the middle.

Quite surprisingly, we find in this paper that braiding of non-Abelian anyons, and hence universal logical gates on encoded qubits, can be performed through a constant depth unitary circuit composed of few-qubit gates acting on the physical qubits. The circuit depth is independent of the separation between the anyons, and thus independent of d. The braiding circuit is composed of a local quantum circuit, $\mathcal{LU}$, which implements a local geometry deformation, and a permutation of qubits, $\mathcal{P}_\sigma: j \mapsto \sigma(j)$, separated by distance of $\mathcal{O}(d)$ and which can be implemented by a depth-2 circuit.

Because of the SolovayKitaev theorem [17], the above result also suggests that arbitrary transformations within the ground state subspace of certain topologically ordered systems supported on a punctured manifold can be realized with a constant-depth unitary circuit independent of the system size, given that the braid group representation of the topological order is computationally universal. Furthermore, our result demonstrates, for the first time, how to construct a universal logical gate set using constant depth unitary circuits, thus circumventing the Eastin-Knill theorem [18], where the long-range permutation is the key to circumvent the assumption in Ref. [18] (see also Ref. [19]). In addition, it also circumvents the no-go's for universality in geometrically local [20] and nonlocal [21] constant-depth circuits, where the circumvention can be mainly attributed to the nonstabilizer nature of the Turaev-Viro codes. Our result can be generalized to arbitrary braids and Dehn twists, which generate the mapping class group of genus g surfaces with n punctures [22–24].

With purely local operations, a unitary circuit that moves non-Abelian anyons or defects over a distance l must have a depth of $\mathcal{O}(l)$ [25]. Abelian anyons, in contrast, can be moved over arbitrary distances in $\mathcal{O}(1)$ time through transversal unitary operations. Our results are thus possible because of the use of long-range permutations in one time step (between two consecutive syndrome measurements), which is naturally suitable for a variety of experimental platforms with long-range connectivity or movable qubits [27–39].

Turaev-viro codes.—We consider Turaev-Viro codes [5,8], which can capture all nonchiral topological states in two dimensions. For the application to universal gate sets we are interested in the doubled Fibonacci state realized by a specific type of Turaev-Viro code. The Turaev-Viro code associates with a closed or punctured surface Σ a finite-dimensional code space $\mathcal{H}_\Sigma$. We use Λ to denote a triangulation of Σ and $\hat{\Lambda}$ to denote the dual cellulation associated with Λ. More specifically, $\hat{\Lambda}$ defines a trivalent graph, such as the honeycomb lattice shown in Fig. 1(a). Each edge of Λ (equivalently, of $\hat{\Lambda}$) is associated with an N-state qudit. If the qudit on a particular edge is in the state $|a\rangle$, we say that there is a string of type a passing through that edge. The wave functions in the code space can be viewed as superpositions of closed *string-net* configurations [8].

The states in the code space are exact ground states of a commuting projector Hamiltonian known as the Levin-Wen Hamiltonian [8], $H_{\hat{\Lambda}} = -\sum_v Q_v - \sum_p B_p$, where v and p label the vertices and plaquettes of $\hat{\Lambda}$. The three-body vertex projection operator Q_v depends only on the three edges incident to v:

$$Q_v \left| \begin{smallmatrix} & a & \\ b & & c \end{smallmatrix} \right\rangle = \delta_{abc} \left| \begin{smallmatrix} & a & \\ b & & c \end{smallmatrix} \right\rangle \tag{1}$$

Here, $\delta_{abc} = 0, 1$ are the branching rules of the allowed string-net configuration. The Fibonacci Turaev-Viro code has $N = 2$ and therefore each edge of the trivalent graph contains two types of strings, as illustrated on the right side of Fig. 1(a), where the edges with (without) the red string correspond to an occupied (unoccupied) site $|1\rangle$ ($|0\rangle$). The branching rules are specified as

$$\delta_{abc} = \begin{cases} 1 & \text{if } abc = 000, 011, 101, 110, 111, \\ 0 & \text{otherwise.} \end{cases} \tag{2}$$

On a honeycomb lattice [Fig. 1(a)], B_p is a 12-body operator that depends on the 6 qubits on the hexagonal plaquette and also on the qubits on the 6 legs connecting to the hexagon. The operator can be written as $B_p = \sum_s d_s B_p^s / D^2$, where d_s is the quantum dimension of the string label s and $D = \sum_s \sqrt{d_s^2}$ is the total quantum dimension. For the Fibonacci code, we have $d_0 = 1$, and $d_1 = \phi = [(\sqrt{5}+1)/2]$. The operator B_p^s is defined via

$$B_p^s \left| \begin{smallmatrix} a & g & & h & c \\ & l & & & i \\ f & & & & \\ & k & & j & \\ & & e & & d \end{smallmatrix} \right\rangle = \sum_{g'h'i'j'k'l'} B_{p,ghijkl,abcdef}^{s,g'h'i'j'k'l'} \left| \begin{smallmatrix} a & g' & & h' & c \\ & l' & & & i' \\ f & & & & \\ & k' & & j' & \\ & & e & & d \end{smallmatrix} \right\rangle,$$

$$B_{p,ghijkl,abcdef}^{s,g'h'i'j'k'l'} = F_{sh'g'}^{bgh} F_{si'h'}^{chi} F_{sj'i'}^{dij} F_{sk'j'}^{ejk} F_{sl'k'}^{fkl} F_{sg'l'}^{alg}.$$

The plaquette operator consists of F symbols, F_{def}^{abc}. The F symbols and the branching rules together define the code. The F symbols also define a controlled-unitary operation; the external a, b, c, d legs are the control qubits that determine the resulting unitary F_d^{abc}, with matrix elements $[F_d^{abc}]_{ef}$.

In the Fibonacci code, the only nontrivial F matrix is

$$F_1^{111} = \begin{pmatrix} \phi^{-1} & \phi^{-\frac{1}{2}} \\ \phi^{-\frac{1}{2}} & -\phi^{-1} \end{pmatrix}. \tag{3}$$

All other F symbols are either 1 or 0, depending on whether they are consistent with the branching rules [Eqs. (2) and (4)]. A quantum circuit implementing the F operations in the Fibonacci code is shown in Fig. 1(b) [40]. The circuit inside the dashed box, consisting of a 5-qubit Toffoli gate sandwiched by two single-qubit rotations, implements the F matrix in Eq. (3). Here, $R_y(\pm\theta) = e^{\pm i\theta\sigma_y/2}$ are single-qubit rotations about the y axis with angle $\theta = \tan^{-1}(\phi^{-\frac{1}{2}})$.

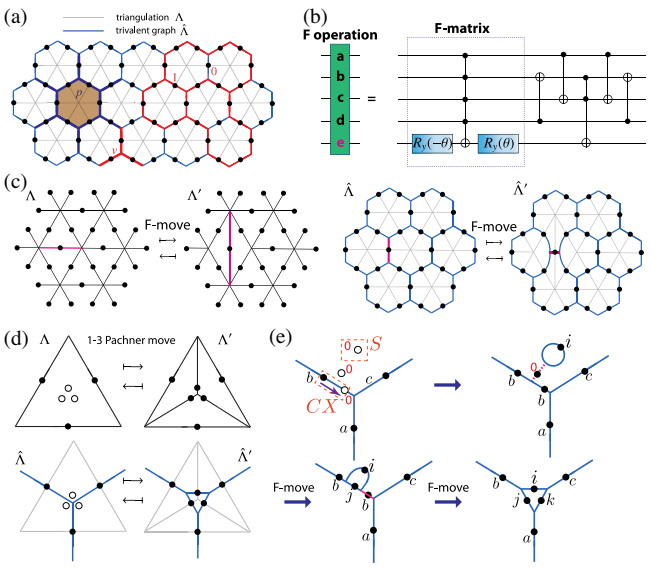

FIG. 1. (a) Definition of the Levin-Wen Hamiltonian on a triangulated manifold. (b) Circuit for F operation in the Fibonacci code. (c) Definition of the 2-2 Pachner move on the triangulation Λ and the corresponding trivalent graph defined by $\hat{\Lambda}$. The pink edges represent the edges being switched during the moves. (d), (e) Definition of the 1-3 Pachner move with the addition or removal of three ancilla qubits (white dots) and the circuit implementation via unitary gates.

All the other maps are taken care of by the rest of the quantum circuit. The Fibonacci code can be implemented by repeated measurements of the vertex and plaquette operators Q_v and B_p [40–43].

Local geometry deformation.—The wave functions in the code space on two different triangulations (dual trivalent graphs) Λ ($\hat{\Lambda}$) and Λ' ($\hat{\Lambda}'$) that differ locally can be related by moves known as 2-2 Pachner moves (also called F moves) and 1-3 Pachner moves, with the following relations:

$$\Psi_{\hat{\Lambda}}\left(\begin{array}{c} b \quad c \\ \quad e \\ a \quad d \end{array}\right) = \sum_f F^{abc}_{def}\, \Psi_{\hat{\Lambda}'}\left(\begin{array}{c} b \quad c \\ \quad f \\ a \quad d \end{array}\right) \tag{4}$$

$$\Psi_{\hat{\Lambda}}\left(\begin{array}{c} b \quad d \quad c \\ \quad e \quad f \\ \quad a \end{array}\right) = [F^{abd}_{fce}]^* \sqrt{\frac{d_d d_f}{d_c}}\, \Psi_{\hat{\Lambda}'}\left(\begin{array}{c} b \quad c \\ \quad a \end{array}\right). \tag{5}$$

Here, $[F^{abd}_{fce}]^*$ denotes the complex conjugate of the elements of the F move defined in Eq. (4), while one has $[F^{abd}_{fce}]^* = F^{abd}_{fce}$ for the Fibonacci code. The local geometry deformation of the triangulation and dual trivalent graph corresponding to the two types of Pachner moves are illustrated in Figs. 1(c), 1(d). Note that the F move preserves the number of qubits (and also their locations) and is obviously a unitary transformation which can be implemented by the conditional circuit in Fig. 1(b). On the other hand, the 1-3 Pachner move adds (entangles) three additional ancilla qubits to the code space, as shown in Fig. 1(d) (from left to right). The reverse process (from right to left) removes (disentangles) three qubits from the code space. Therefore, the 1-3 Pachner move can be related to entanglement renormalization performing either fine-graining or coarse-graining of the lattice, which has been studied in the context of MERA (multiscale entanglement renormalization ansatz) of string nets [15,16].

Taking into account the additional qubits, the 1-3 Pachner move can also be implemented by a sequence of unitary gates as illustrated in Fig. 1(e). We first consider three extra qubits, each initialized to the $|0\rangle$ state. Next, we apply a CNOT (indicated by the purple arrow), which takes $|b\rangle|0\rangle \mapsto |b\rangle|b\rangle$. This is equivalent to an isometry in the MERA language. At the same time, we apply modular $S{:}\,|0\rangle \mapsto \sum_i (d_i/D)|i\rangle$ to the top-most qubit [44], which effectively builds a "tadpole diagram" connected to the original graph through the edge with the remaining ancilla in the $|0\rangle$ state. Note that the original edge labeled by b is split into two edges with the same label b. Next, we apply two successive F moves and hence end up with the desired trivalent graph with a triangular plaquette replacing the original vertex in the center. This process is reversible.

Moving anyons in constant time.—An intuitive way to understand the moving protocol is through the picture of local entanglement renormalization. The essence of entanglement renormalization and the MERA circuit can be understood as a global coarse graining (fine-graining) process that "merges" ("splits") several qubits together, effectively removing (adding) qubits in the code, as illustrated in Fig. 2(a). In the context of topological order, one can think of this process as squeezing (stretching) the manifold which supports the topological states. Now one can consider anyons or defects as punctures (yellow circles) in the manifold as illustrated in the lower panel. In order to separate two adjacent punctures to distance d, one needs a MERA circuit with depth (layers) $\log_2(d)$, where each step stretches the manifold by a factor of 2. When the two punctures are already separated by a distance d, one can perform one layer of the local entanglement renormalization circuit (with constant depth) to stretch (fine-grain) the region between the two punctures to increase the distance to $2d$, which effectively adds qubits into the system, as illustrated in Fig. 2(b). Now the manifold is effectively enlarged due to the addition of qubits. In order to preserve the shape of the manifold away from the region of the punctures, one can also perform one layer of local entanglement renormalization to squeeze (coarse-grain) the region on the left and right sides of the punctures, as shown in Fig. 2(c). Thus one effectively ends up with the same overall shape of the manifold, with the two punctures being separated by a factor of 2, i.e., $d \to 2d$. Note that according to the left panel of Fig. 2(c), in order to map the qubit lattice exactly to the original shape, one performs SWAPs (green arrows indicated in the bottom layer) with largest distance of $\mathcal{O}(d)$. The long-range SWAP ensures that the actual location of each puncture is moved by a distance $d/2$.

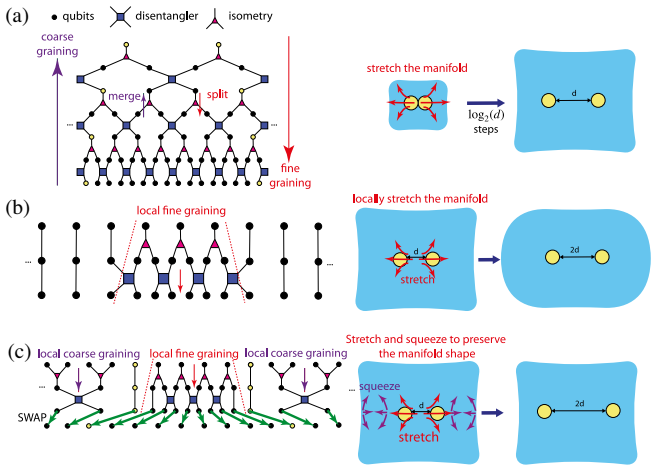

FIG. 2. Understanding the essence of braiding via the equivalence of local entanglement renormalization and manifold stretching/squeezing. (a) MERA is equivalent to stretching the manifold in $\log_2(d)$ steps. (b) Local entanglement renormalization is equivalent to stretching the manifold in a single step. (c) Locally squeeze the rest of the region in a single step to preserve the overall shape of the manifold.

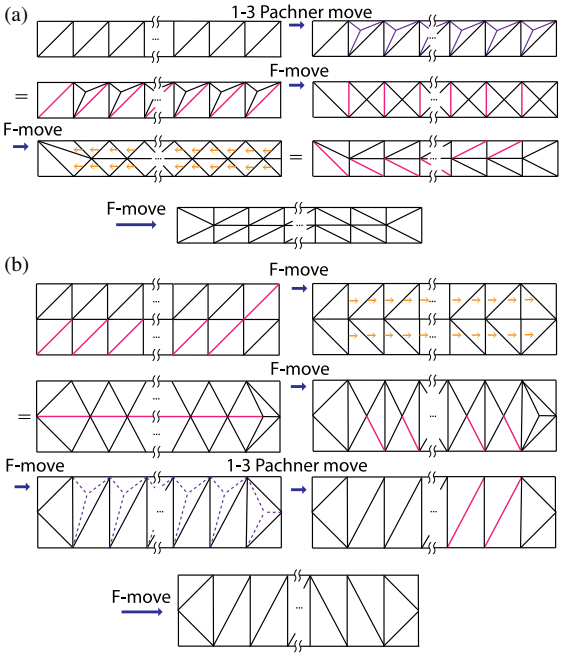

FIG. 3. Gadgets for local geometry deformation in Turaev-Viro codes. The solid (dashed) purple lines represent added (removed) edges during the 1-3 Pachner moves. The yellow arrow indicates the equivalence between two triangulations. (a) Fine-grain the lattice via splitting a single row into two in a bounded region. (b) Coarse-grain the lattice via merging two rows into one.

Constant-depth braiding circuit.—For the implementation of braiding, we need to introduce two elementary gadgets, as illustrated in Fig. 3. In Fig. 3(a), we consider triangulation of a single row of arbitrary length. By utilizing ancilla qubits, we can implement the 1-3 Pachner moves, which increase the number of vertices of the triangulation. By a finite sequence of F moves and local SWAPs, we can effectively split a single row of arbitrary length L into two rows, with a constant (independent of L) number of steps (i.e., a constant depth local unitary circuit). In Fig. 3(b), we illustrate how two rows can be converted into a single row by a finite number of steps. Note that in both protocols, the qubits on the outer boundary of the rows shown are completely unaffected, acting as control qubits for the unitary operations, allowing the transformations to be applied to all rows in parallel.

Using the above gadgets, we can now demonstrate our braiding circuit on a triangulated region (Fig. 4). First, in the region between anyon I and III, we split rows of varying lengths in two rows, while combining rows in the region above the anyon [Fig. 4(b)]. We create a lattice Λ' with a shearing pattern on the left and right sides of anyon I; the regions above anyon I being coarse grained (squeezed) while the region below it is fine grained (stretched). Now via long-range permutation of qubits (green arrows) $\mathcal{P}_\sigma$, where $\mathcal{P}_\sigma$ is the unitary representation of the permutation σ, we reach the configuration in Fig. 4(c) which is isomorphic to the configuration in Fig. 4(b), with anyon I being moved up

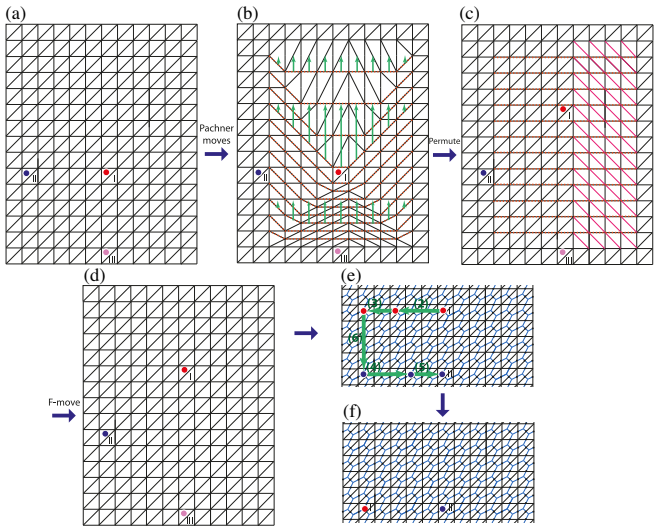

FIG. 4. (a)–(f) Braiding of two non-Abelian anyons in Turaev-Viro codes with constant-depth circuit. The orange dashed lines in (b) and (c) show the equivalent edges before/after the permutation. Each green arrow in (e) corresponds to an instantaneous moving (number specifying the order) carried out by an analogous procedure described in panels (a)–(d).

in space. To recover the original triangulation Λ, we apply another retriangulation in the strip on the right of anyon I (pink thick lines), thus mapping back to the original lattice in Fig. 4(d).

The above protocol, using a constant-depth local quantum circuit and long-range qubit permutations, effectively moves one anyon vertically by a distance of the order of the separation between the nearest anyon II (on the order of the code distance d). The (vertical) separation between anyon I and III is also increased by a factor of 2, which concretely demonstrates the local entanglement renormalization idea in Fig. 2(c). To complete a braiding cycle, we apply another 5 shots of a similar procedure, which then effectively braid anyons I and II around each other as illustrated in Figs. 4(e),(f). Here, we show the qubits (black dots) and trivalent graph (light blue lines) explicitly for concreteness.

The permutations can be applied through a constant depth circuit in a variety of ways. For example, arbitrary permutations can always be implemented by a depth-two circuit, where each layer corresponds to long-range SWAP operations applied in parallel. This can be seen by noting that an arbitrary permutation of objects can be written as a product of cyclic permutations over disjoint sets. A cyclic permutation can always be performed in two steps, where each step corresponds to SWAP operations applied in parallel.

To summarize, a single braiding operation can be performed in a constant number of steps, independent of the system size and code distance. This is in contrast to previous computation schemes for the Turaev-Viro code in Ref. [5], where braiding or Dehn twists are implemented by sequential F moves with circuit depth of $\mathcal{O}(d)$. Here we have demonstrated a six-step procedure:

$$\mathcal{B}_{\mathrm{I,II}} = \prod_{i=1}^{6} \mathcal{LU}_i' \mathcal{P}_{\sigma,i} \mathcal{LU}_i. \tag{6}$$

Each step is composed of a constant-depth local quantum circuit $\mathcal{LU}_i$ corresponding to a retriangulation of the manifold, a permutation of qubits $\mathcal{P}_{\sigma,i}$ over a distance $\mathcal{O}(d)$, and another local circuit $\mathcal{LU}_i'$ in order to retriangulate the manifold back to the original triangulation.

We emphasize that our protocols are constant depth unitary circuits, which neither depend on the results of any measurement outcomes nor introduce plaquette or vertex operators whose measurement outcomes are unknown. This makes our protocols fundamentally distinct from other proposed methods for logical operations in stabilizer codes, such as lattice surgery methods or certain schemes for moving non-Abelian defects in Abelian stabilizer codes, e.g., in Ref. [3]. Therefore, no classical communication or classical computation is required and thus our protocols are truly constant depth both in terms of quantum operations and classical computation.

Topological protection and fault tolerance aspects.—The constant-depth logical gates (denoted by U) developed here are naturally topologically protected (and thus can be made fault tolerant) since a local operator O with support in a region $\mathcal{R}$ is mapped to another local operator $U^\dagger O U$ supported in a region $\mathcal{R}'$ such that the area ratio of $\mathcal{R}'$ and $\mathcal{R}$ is bounded by an $\mathcal{O}(1)$ constant factor c, similar to the property of a locality-preserving unitary [45,46], i.e., $\mathsf{supp}(U^\dagger O U) \leq c\mathsf{supp}(O)$. This is due to the constant depth of the local unitary circuits and the specific form of the permutations we used. As a result, the circuit only changes the length of error strings by an $\mathcal{O}(1)$ constant factor independent of code distance d. Therefore, any local error string with length much less than d remains local during the protocol and can not access the non-locally encoded logical information [47].

After the application of each logical gate, the extra time overhead due to decoding and error correction depends on the details of the logical circuit of the target quantum algorithm. In the cases when the length of the error string does not increase or increases linearly, the situation is analogous to a constant-depth local quantum circuit [20] and only $\mathcal{O}(1)$ rounds of syndrome measurement per logical gate is expected, leading to a constant time overhead. In the worst-case scenario, when certain sequence of braids are repetitively applied in the same region and the error string is always stretched by a constant factor, the error string will grow to the code distance in $\log d$ time steps. To prevent this, $\mathcal{O}(d)$ rounds of measurement needs to be inserted for every $\log d$ logical gates in the presence of measurement noise to decode the error syndrome. Therefore, we estimate that there is an $\mathcal{O}(d/\log d)$ time overhead in the generic case to achieve full fault tolerance, although a detailed decoding scheme needs to be further developed to verify this estimation. Because of the strictly bounded operator support of our logical gates (Fig. 4), one also expects that certain highly sequential logical circuits can also have $\mathcal{O}(1)$ time overhead, when any given physical qubit is only acted on by $\mathcal{O}(1)$ operators in $\mathcal{O}(d)$ time steps (such that d rounds of measurement can be applied to decode the error syndrome before the error string is further stretched).

We thank M. Freedman, J. Preskill, M. Hastings, J. Haah, M. Hafezi, Z. Wang, and S. Jordan for helpful discussions. This work was supported by NSF CAREER (DMR-1753240), JQI-PFC-UMD (Joint Quantum Institute-Physics Frontier Center-University of Maryland), ARO-MURI (Multidisciplinary University Research Initiative), and (Young Investigator Program) YIP-ONR.

[1] B. M. Terhal, Rev. Mod. Phys. **87**, 307 (2015).
[2] E. T. Campbell, B. M. Terhal, and C. Vuillot, Nature **529**, 172 (2017).
[3] A. G. Fowler, M. Mariantoni, J. M. Martinis, and A. N. Cleland, Phys. Rev. A **86**, 032324 (2012).
[4] A. Kitaev, Ann. Phys. (Amsterdam) **303**, 2 (2003).
[5] R. Koenig, G. Kuperberg, and B. W. Reichardt, Ann. Phys. (Amsterdam) **325**, 2707 (2010).
[6] M. Barkeshli, P. Bonderson, M. Cheng, and Z. Wang, Phys. Rev. B **100**, 115147 (2019).
[7] I. Cong, M. Cheng, and Z. Wang, arXiv:1609.02037.
[8] M. A. Levin and X.-G. Wen, Phys. Rev. B **71**, 045110 (2005).
[9] M. H. Freedman, M. Larsen, and Z. H. Wang, Commun. Math. Phys. **227**, 605 (2002).
[10] Z. Wang, *Topological Quantum Computation* (American Mathematics Society, Providence, 2010).
[11] N. E. Bonesteel, L. Hormozi, G. Zikos, and S. H. Simon, Phys. Rev. Lett. **95**, 140503 (2005).
[12] S. Bravyi and A. Kitaev, Phys. Rev. A **71**, 022316 (2005).
[13] A. Paetznick and B. W. Reichardt, Phys. Rev. Lett. **111**, 090505 (2013).
[14] H. Bombin, New J. Phys. **17**, 083002 (2015).
[15] G. Vidal, Phys. Rev. Lett. **99**, 220405 (2007).
[16] R. König, B. W. Reichardt, and G. Vidal, Phys. Rev. B **79**, 195123 (2009).
[17] M. A. Nielsen and I. L. Chuang, *Quantum Computation and Quantum Information: 10th Anniversary Edition* (Cambridge University Press, Cambridge, England, 2010).
[18] B. Eastin and E. Knill, Phys. Rev. Lett. **102**, 110502 (2009).
[19] B. Zeng, A. Cross, and I. L. Chuang, IEEE Trans. Inf. Theory **57**, 6272 (2011).
[20] S. Bravyi and R. König, Phys. Rev. Lett. **110**, 170503 (2013).
[21] T. Jochym-O'Connor, A. Kubica, and T. J. Yoder, Phys. Rev. X **8**, 021047 (2018).
[22] G. Zhu, M. Hafezi, and M. Barkeshli, Phys. Rev. Research **2**, 013285 (2020).
[23] G. Zhu, A. Lavasani, and M. Barkeshli, arXiv:1806.06078.
[24] This includes the case of transformation between arbitrary ground states supported on a closed manifold.
[25] We note that our result here is about using unitary circuits to instantaneously move non-Abelian anyons or defects. It is

known that, without measurement errors, one can move non-Abelian twist and hole defects in Abelian topological stabilizer codes instantaneously through measurements (nonunitary) [3,26]. Nevertheless, even without measurement error, it is not known how to move non-Abelian anyons instantaneously through measurements.

[26] B. J. Brown, K. Laubscher, M. S. Kesselring, and J. R. Wootton, Phys. Rev. X **7**, 021029 (2017).

[27] N. M. Linke, D. Maslov, M. Roetteler, S. Debnath, C. Figgatt, K. A. Landsman, K. Wright, and C. Monroe, Proc. Natl. Acad. Sci. U.S.A. **114**, 3305 (2017).

[28] R. Bowler, J. Gaebler, Y. Lin, T. R. Tan, D. Hanneke, J. D. Jost, J. P. Home, D. Leibfried, and D. J. Wineland, Phys. Rev. Lett. **109**, 080502 (2012).

[29] K. Wright, J. M. Amini, D. L. Faircloth, C. Volin, S. C. Doret, H. Hayden, C.-S. Pai, D. W. Landgren, D. Denison, T. Killian *et al.*, New J. Phys. **15**, 033004 (2013).

[30] J. P. Home, D. Hanneke, J. D. Jost, J. M. Amini, D. Liebfried, and D. J. Wineland, Science **325**, 1227 (2009).

[31] B. Lekitsch, S. Weidt, A. G. Fowler, K. Mølmer, S. J. Devitt, C. Wunderlich, and W. K. Hensinger, Sci. Adv. **3**, e1601540 (2017).

[32] P. Campagne-Ibarcq, E. Zalys-Geller, A. Narla, S. Shankar, P. Reinhold, L. D. Burkhart, C. J. Axline, W. Pfaff, L. Frunzio, R. J. Schoelkopf *et al.*, Phys. Rev. Lett. **120**, 200501 (2018).

[33] P. Kurpiers, P. Magnard, T. Walter, B. Royer, M. Pechal, J. Heinsoo, Y. Salathé, A. Akin, S. Storz, J.-C. Besse *et al.*, Nature **558**, 264 (2018).

[34] C. Axline, L. Burkhart, W. Pfaff, M. Zhang, K. Chou, P. Campagne-Ibarcq, P. Reinhold, L. Frunzio, S. M. Girvin, L. Jiang *et al.*, Nat. Phys. **14**, 705 (2019).

[35] K. S. Chou, J. Z. Blumoff, C. S. Wang, Reinhold, P. C., C. J. Axline, Y. Y. Gao, L. Frunzio, M. H. Devoret, L. Jiang, and R. J. Schoelkopf, Nature **561**, 368 (2018).

[36] J. Majer, J. M. Chow, J. M. Gambetta, J. Koch, B. R. Johnson, J. A. Schreier, L. Frunzio, D. I. Schuster, A. A. Houck, A. Wallraff *et al.*, Nature (London) **449**, 443 (2007).

[37] F. Helmer, M. Mariantoni, A. G. Fowler, J. von Delft, E. Solano, and F. Marquardt, Europhys. Lett. **85**, 50007 (2009).

[38] R. K. Naik, N. Leung, S. Chakram, P. Groszkowski, Y. Lu, N. Earnest, D. C. McKay, J. Koch, and D. I. Schuster, Nat. Commun. **8**, 1904 (2017).

[39] D. A. Herrera-Martí, A. G. Fowler, D. Jennings, and T. Rudolph, Phys. Rev. A **82**, 032332 (2010).

[40] N. E. Bonesteel and D. P. DiVincenzo, Phys. Rev. B **86**, 165113 (2012).

[41] W. Feng, Non-Abelian quantum error correction, Ph.D. thesis, Florida State University, 2015.

[42] S. Burton, C. G. Brell, and S. T. Flammia, Phys. Rev. A **95**, 022309 (2017).

[43] G. Dauphinais and D. Poulin, Commun. Math. Phys. **355**, 519 (2017).

[44] In the context of the Fibonacci code, the modular S gate is a single qubit rotation which can be represented by $S = [1/(\sqrt{2+\phi})]\left(\begin{smallmatrix} 1, & \phi \\ \phi, & -1 \end{smallmatrix}\right)$.

[45] The difference with the definition of the locality-preserving unitary used in Ref. [46] is that in our case $\mathcal{R}$ and $\mathcal{R}'$ do not have to be located near each other.

[46] M. E. Beverland, O. Buerschaper, R. Koenig, F. Pastawski, J. Preskill, and S. Sijher, J. Math. Phys. (N.Y.) **57**, 022201 (2016).

[47] See Supplemental Material at http://link.aps.org/supplemental/10.1103/PhysRevLett.125.050502 for discussion of topological protection, fault-tolerant aspects and overall time complexity, and experimental platforms.